Pressure effect on the anomalous Hall effect of ferromagnetic Weyl semimetal $Co_3Sn_2S_2$

Z. Y. Liu,[1,2,*] T. Zhang,[1,3,*] S. X. Xu,[1,3] P. T. Yang,[1,3] Q. Wang,[4] H. C. Lei,[4] Y. Sui,[2] Y. Uwatoko,[5] B. S. Wang,[1,3,6] H. M. Weng,[1,3,6,7,†] J. P. Sun,[1,3,‡] and J.-G. Cheng[1,3,6]

[1]*Beijing National Laboratory for Condensed Matter Physics and Institute of Physics, Chinese Academy of Sciences, Beijing 100190, China*
[2]*School of Physics, Harbin Institute of Technology, Harbin 150001, China*
[3]*School of Physical Sciences, University of Chinese Academy of Sciences, Beijing 100190, China*
[4]*Department of Physics and Beijing Key Laboratory of Opto-electronic Functional Materials & Micro-nano Devices, Renmin University of China, 100872 Beijing, China*
[5]*Institute for Solid State Physics, University of Tokyo, Kashiwa, Chiba 277–8581, Japan*
[6]*Songshan Lake Materials Laboratory, Dongguan, Guangdong 523808, China*
[7]*CAS Center for Excellence in Topological Quantum Computation, University of Chinese Academy of Sciences, Beijing 100190, China*

(Received 11 December 2019; accepted 9 April 2020; published 28 April 2020)

The magnetic Weyl semimetal $Co_3Sn_2S_2$ exhibits large anomalous Hall effect (AHE) due to its nontrivial band topology with enhanced Berry curvature. Here we investigate the pressure effect on the AHE of $Co_3Sn_2S_2$ up to 12 GPa with a palm cubic anvil cell apparatus and first-principles calculations simulation. We find that both the ferromagnetic transition temperature and the AHE are suppressed monotonically upon the application of high pressure. Data analyses revealed that in the investigated pressure range the intrinsic mechanism due to Berry curvature dominates the AHE as reflected by the validation of $\rho_{xy}^A \propto \rho_{xx}^2$. However, both the anomalous Hall conductivity and anomalous Hall angle are reduced gradually into the regime for conventional ferromagnetic metals with trivial band topology. Combined with theoretical calculations, our results indicate that the distance between Weyl points with opposite chirality in $Co_3Sn_2S_2$ is substantially reduced accompanying the suppression of ferromagnetism by pressure, thus providing an experimental route to tune the AHE of magnetic Weyl semimetals via modifying the nontrivial band topology.

DOI: 10.1103/PhysRevMaterials.4.044203

I. INTRODUCTION

Recently, the combination/interplay of magnetism and nontrivial electronic band topology in a single-phase compound has emerged as an exciting research field for exploring exotic topological quantum phenomena [1–6]. For example, the intrinsic magnetic topological insulators might realize quantum anomalous Hall effect at elevated temperatures, while the magnetic Weyl semimetals with broken time-reversal symmetry are expected to generate giant intrinsic anomalous Hall effect (AHE) due to the large Berry curvature [7–10]. The layered $MnBi_2Te_4$ has been proposed as the first candidate of intrinsic magnetic topological insulators [5,11–13], and several important progresses have been achieved recently [14–22]. On the other hand, $Co_3Sn_2S_2$ with a Shandite-type structure has been established recently as a magnetic Weyl semimetal with giant intrinsic AHE [23–25].

The latter compound $Co_3Sn_2S_2$ adopts a rhombohedral crystal structure with space group *R-3m* (No. 166); the Co atoms are octahedrally coordinated by two S and four Sn atoms and form perfect kagome layers that are stacked along the *c* axis [23,24,26]. Measurements of magnetic properties reveal that $Co_3Sn_2S_2$ undergoes a long-range ferromagnetic (FM) order below $T_C \approx 177$ K with a dominant out-of-plane magnetic anisotropy. The measured saturation moment of $\sim 0.3\,\mu_B$/Co below T_C is substantially smaller than the effective paramagnetic moment of $1.15\,\mu_B$, signaling an itinerant-electron ferromagnetism in this system [27]. Accordingly, its longitudinal resistivity $\rho_{xx}(T)$ exhibits a metallic behavior with a clear kink anomaly at T_C. Band structure calculations indicate a half-metallic character for $Co_3Sn_2S_2$ at the FM state [23,24,28–32]. In the absence of spin-orbit coupling (SOC), there exist mirror-symmetry protected linear band crossings along high symmetry lines for the spin-up channel; they will decay into a pair of Weyl points with opposite chirality when the SOC is included [23,24]. It has been well established very recently that $Co_3Sn_2S_2$ is a magnetic Weyl semimetal hosting emergent Weyl fermions in the bulk and surface Fermi arcs state that connects the Weyl points of opposite chirality [33–35]. As a result of time-reversal symmetry (TRS) breaking in the magnetic Weyl semimetal state, both large anomalous Hall conductivity and giant anomalous Hall angle are observed below T_C of $Co_3Sn_2S_2$, making it promising for spintronics applications [23,24].

Since the TRS breaking magnetic Weyl semimetal state and intrinsic AHE in $Co_3Sn_2S_2$ are intimately correlated with the ferromagnetism, it is desirable to further manipulate the magnetism and to investigate their relationship. In this regard, high pressure (HP) can be employed as an effective and clean means, especially for the itinerant-electron ferromagnets like $Co_3Sn_2S_2$. According to the theoretical

*These authors contributed equally to this work.
†hmweng@iphy.ac.cn
‡jpsun@iphy.ac.cn

calculations, the anomalous Hall conductivity of $Co_3Sn_2S_2$ will decrease gradually upon the reduction of the magnetic moment of cobalt because the distance between Weyl points with opposite chirality also shows a monotonic decrease [24]. In a recent comprehensive HP study, however, it was shown that while the FM order and the magnetic moment decrease monotonically with pressure, the anomalous Hall conductivity of $Co_3Sn_2S_2$ varies nonmonotonically against pressure, *i.e.* it first increases from 0.2 to 4.9 GPa and then decreases abruptly upon further compression [36]. Whether such a discrepancy is an intrinsic effect of pressure or arises from some extrinsic factors deserves further studies. As pointed out in the above study, the observed coercive field H_C under pressure is 2–4 times larger than that at ambient pressure [36]. This has been ascribed to the disorder or stress gradient experienced by sample in the diamond anvil cell because a solid NaCl pressure transmitting medium was used in the HP transport experiments. Therefore, a more dedicated HP study with improved pressure homogeneity is desirable.

In this work, we have employed the cubic anvil cell to study the pressure effect on the AHE of $Co_3Sn_2S_2$ up to 12 GPa. In comparison with diamond anvil cell, the cubic anvil cell can maintain a better pressure homogeneity due to the adoption of three-axis compression geometry and the liquid pressure transmitting medium. We find that both the FM transition temperature and the AHE are suppressed monotonically upon the application of HP. Although the intrinsic mechanism due to Berry curvature still dominates the AHE as reflected by the validation of $\rho_{xy}^A \propto \rho_{xx}^2$, both the anomalous Hall conductivity and anomalous Hall angle are reduced monotonically into the regime for conventional FM metals with trivial band topology. In agreement with the theoretical calculations, our results indicate that the distance between Weyl points with opposite chirality is substantially reduced accompanying the suppression of ferromagnetism in $Co_3Sn_2S_2$ under HP, thus providing an experimental route to tune the large AHE of magnetic Weyl semimetals.

II. EXPERIMENTS AND CALCULATION METHODS

$Co_3Sn_2S_2$ single crystals used in present study were grown out of the Sn flux. Details about the crystal growth and sample characterizations at ambient pressure have been published elsewhere [24]. HP magnetotransport measurements were performed in the palm cubic anvil cell apparatus. Both longitudinal resistivity ρ_{xx} and Hall resistivity ρ_{xy} were measured by the standard four-probe method with the current applied within the *ab* plane and the magnetic field along the *c* axis. The $\rho_{xy}(H)$ data were antisymmetrized with respect to the magnetic field between + 0.5 and − 0.5 T. We used glycerol as the pressure transmitting medium and the characteristic transitions of bismuth and lead to calibrate pressure values at room temperature. Details about the sample assembly and pressure calibrations can be found in our previous publications [37,38].The first-principles simulations of $Co_3Sn_2S_2$ are performed by using the Vienna *ab initio* simulation package (VASP) [39] with the generalized gradient approximation (GGA) of Perdew-Burke-Ernzerhof (PBE) exchange correlation potential [40–42]. The cutoff energy is 400 eV and the reciprocal space is sampled by 11 × 11 × 11 Γ-centered *k* mesh. The SOC is taken into account in self-consistent band calculations. The pressure effects are simulated by varying either the magnetic moment of Co atoms or the lattice constants obtained from the HP magnetization and XRD measurements [36]. The lattice constants are $a = b = 5.3724$ Å and $c = 13.1972$ Å at ambient pressure, and the atom positions have been relaxed for different lattice constants. In order to further calculate the intrinsic anomalous Hall conductivity of $Co_3Sn_2S_2$, we construct the tight-binding Hamiltonian for Co 3*d*, Sn 5*p*, and S 3*p* orbitals by using WANNIER 90 package [43,44]. The intrinsic anomalous Hall conductivity are gained according to the formula in Ref. [24] with 100 × 100 × 100 *k*-point grids based on the tight-binding Hamiltonian by the WANNIERTOOLS package [45].

III. RESULTS AND DISCUSSIONS

Figure 1(a) displays the zero-field resistivity $\rho(T)$ for $Co_3Sn_2S_2$ under various pressures up to 12 GPa. In agreement with previous reports [23,24], the $\rho(T)$ at ambient pressure shows a metallic behavior with a clear kink anomaly at the FM transition temperature $T_C = 174$ K, which is defined simply from the interception between two straight lines below and above the kink anomaly. With increasing pressure, the magnitude of $\rho(T)$ is reduced gradually, but the overall behavior of metallic $\rho(T)$ keeps essentially similar. The absence of sudden change of resistivity upon compression to 12 GPa is consistent with the absence of structural transition in the investigated pressure range [36]. Meanwhile, the T_C manifested by the kink anomaly in resistivity is lowered monotonically to ∼90 K at 12 GPa. These results are in generally consistent with the recent HP study by Chen *et al.* [36] However, it should be noted that the kink anomaly in resistivity at T_C remains well resolved up to 12 GPa in the present study, whereas it can be hardly discerned under pressures in Ref. [36]. This comparison elaborates a better pressure homogeneity of cubic anvil cell used in the present study.

Figure 1(b) displays the pressure dependence of $T_C(P)$ determined from two runs of HP $\rho(T)$ measurements in the present study together with that from HP $M(T)$ data in Ref. [36]. These data are in general consistent with each other, and illustrate a continuous suppression of T_C with a linear slope of $dT_C/dP \sim -8$ K/GPa. A linear extrapolation of $T_C(P)$ would predict a putative critical pressure of $P_c \sim$ 22 GPa for the complete suppression of the FM order. In general, the itinerant-electron ferromagnetism can be suppressed by pressure because the electronic bandwidth is broadened up and the exchange splitting weakened. In comparison with typical itinerant-electron ferromagnets such as $ZrZn_2$ and MnSi, however, the critical pressure of $Co_3Sn_2S_2$ is nearly an order of magnitude higher [36,46,47]. Considering the relatively small moment of 0.3 μ_B/Co, such a robustness of ferromagnetism under pressure in $Co_3Sn_2S_2$ is quite unusual and might have a deep root in the half-metallicity and nontrivial band topology, which is further elaborated by the band-structural calculations under HP shown below. On the other hand, the FM transition in $Co_3Sn_2S_2$ might be enhanced if a negative chemical or physical pressure can be applied, which deserves further studies.

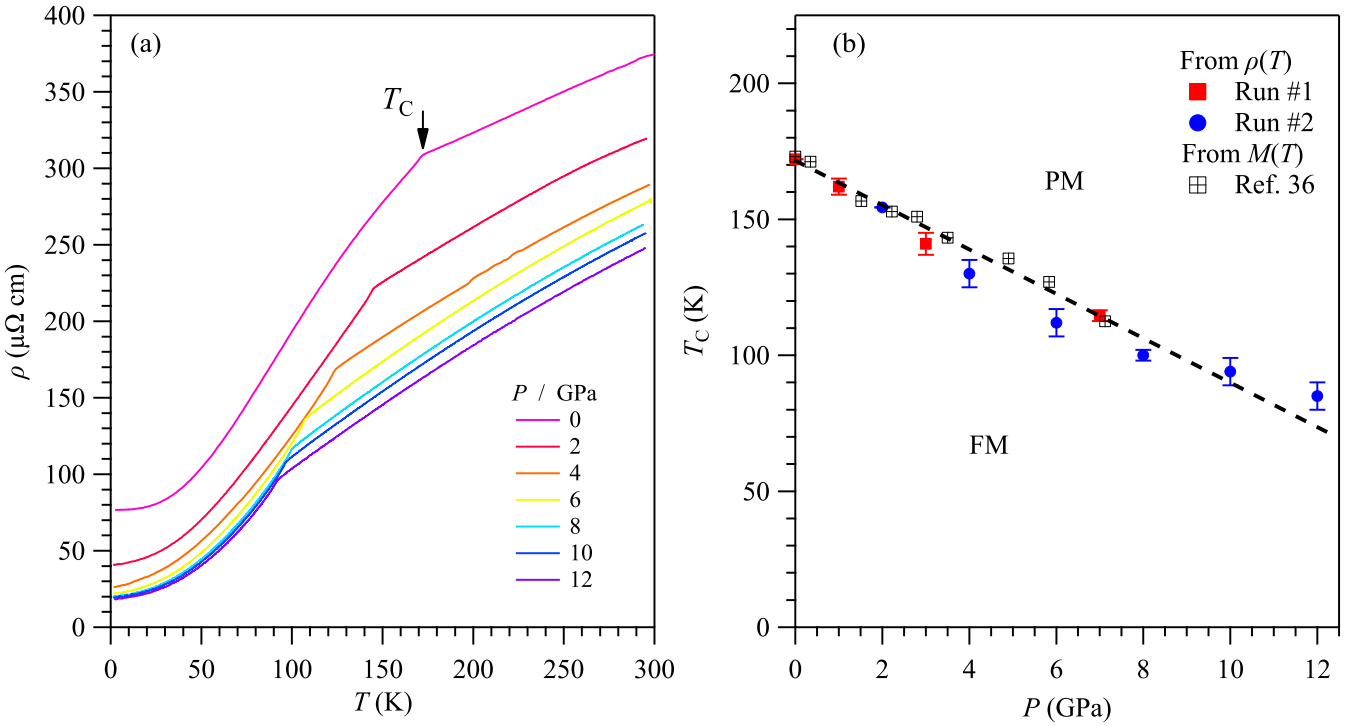

FIG. 1. (a) Temperature dependence of zero-field resistivity $\rho(T)$ of $Co_3Sn_2S_2$ under various pressures up to 12 GPa. (b) Pressure dependence of the ferromagnetic transition temperature T_C of $Co_3Sn_2S_2$. The PM and FM represent for paramagnetism and ferromagnetism.

To evaluate the pressure effect on the AHE of $Co_3Sn_2S_2$, we measured Hall resistivity $\rho_{xy}(H)$ at different temperatures under each pressure. All data are shown in Fig. 2. As can be see, the $\rho_{xy}(H)$ data at each pressure share similar features as those at ambient pressure [24]. In specific, $\rho_{xy}(H)$ curves at $T < T_C$ display a clear hysteresis loop with a sizable jump, characteristic of AHE. The coercive filed H_C decreases gradually with increasing temperature to T_C, while the saturation value of ρ_{xy} exhibits a nonmonotonic variation with temperature, reaching the maximum at a temperature lower than T_C as shown below. With increasing pressure, the maximum saturation value of ρ_{xy} below T_C decreases gradually, from over 20 $\mu\Omega$ cm at ambient pressure to about 15 $\mu\Omega$ cm at 2 GPa, and finally to < 1.5 $\mu\Omega$ cm at 12 GPa. In comparison with the results in Ref. [36], there are some differences. For example, the coercive field remains comparable to that at ambient pressure, e.g., $H_C \sim 0.1$ T at 2 K up to 12 GPa, further elaborating an excellent pressure homogeneity in the present study. In addition, we did not observe the negative slope of Hall resistivity up to 12 GPa.

As we know, the Hall resistivity $\rho_{xy}(H)$ below T_C of magnetic materials includes two parts, i.e., $\rho_{xy} = \rho_{xy}{}^{O} + \rho_{xy}{}^{A}$, where $\rho_{xy}{}^{O} = R_H \times B$ is the ordinary Hall resistivity due to Lorentz force with R_H the Hall coefficient, and $\rho_{xy}{}^{A}$ is the anomalous Hall resistivity [7]. Here we determine $\rho_{xy}{}^{A}$ below T_C by extrapolating a linear fitting of $\rho_{xy}(H)$ to zero field for further discussions. Figure 3(a) displays the temperature dependence of $\rho_{xy}{}^{A}$ at different pressures. As can be seen, $\rho_{xy}{}^{A}(T)$ at each pressure exhibits a broad peak at $T^{max} < T_C$; both the magnitude and T^{max} of the peak shift to lower temperatures with increasing pressure. The maximum value of $\rho_{xy}{}^{A}$ decreases by one order of magnitude from ~15 $\mu\Omega$ cm at 2 GPa to ~1.5 $\mu\Omega$ cm at 12 GPa. To check if the intrinsic mechanism of Berry curvature still holds, we have plotted $\rho_{xy}{}^{A}$ versus ρ_{xx} below T_C in a double logarithmic scale in Fig. 3(b). A linear fitting was employed to deduce the exponent α according to the formula $\rho_{xy}{}^{A} \propto \rho_{xx}{}^{\alpha}$. As illustrated in Fig. 3(b), the obtained α keeps at an essentially constant value of 2 ± 0.1, suggesting that the intrinsic mechanism due to Berry curvature still dominates the AHE at least up to 12 GPa despite of the strong suppression of $\rho_{xy}{}^{A}$.

To substantiate the intrinsic mechanism of AHE, we further deduce the anomalous Hall conductivity $\sigma_{xy}{}^{A} \equiv \rho_{xy}{}^{A}/[(\rho_{xy}{}^{A})^2 + (\rho_{xx})^2]$ at different pressures and displayed in Figs. 3(c) and 3(d) as a function of temperature T and σ_{xx}, respectively. As shown in Fig. 3(c), $\sigma_{xy}{}^{A}(T)$ is nearly independent of temperature below 50 K, which is consistent with that at ambient pressure. Such a behavior becomes more prominent under higher pressures. As can be seen, both temperature and pressure can destruct the ferromagnetic order and suppress the anomalous Hall conductivity, but their effects are realized in different ways. For the temperature effect, it is induced by the competition between the potential energy of correlated electrons and the total kinetic energy. While under high pressures, it is the changes of the interactions between the localized d-orbital states and the hybridizations between different orbital states that lead to a change of the polarized band structure and a suppression of the anomalous Hall conductivity. In addition, we can see in Fig. 3(d) that for all pressures $\sigma_{xy}{}^{A}$ is nearly independent of σ_{xx} below T_C, and the conductivity of $Co_3Sn_2S_2$ situates in an intermediate metallic regime with $10^4 < \sigma_{xx} < 10^6$ $\mu\Omega^{-1}$ cm^{-1}. All

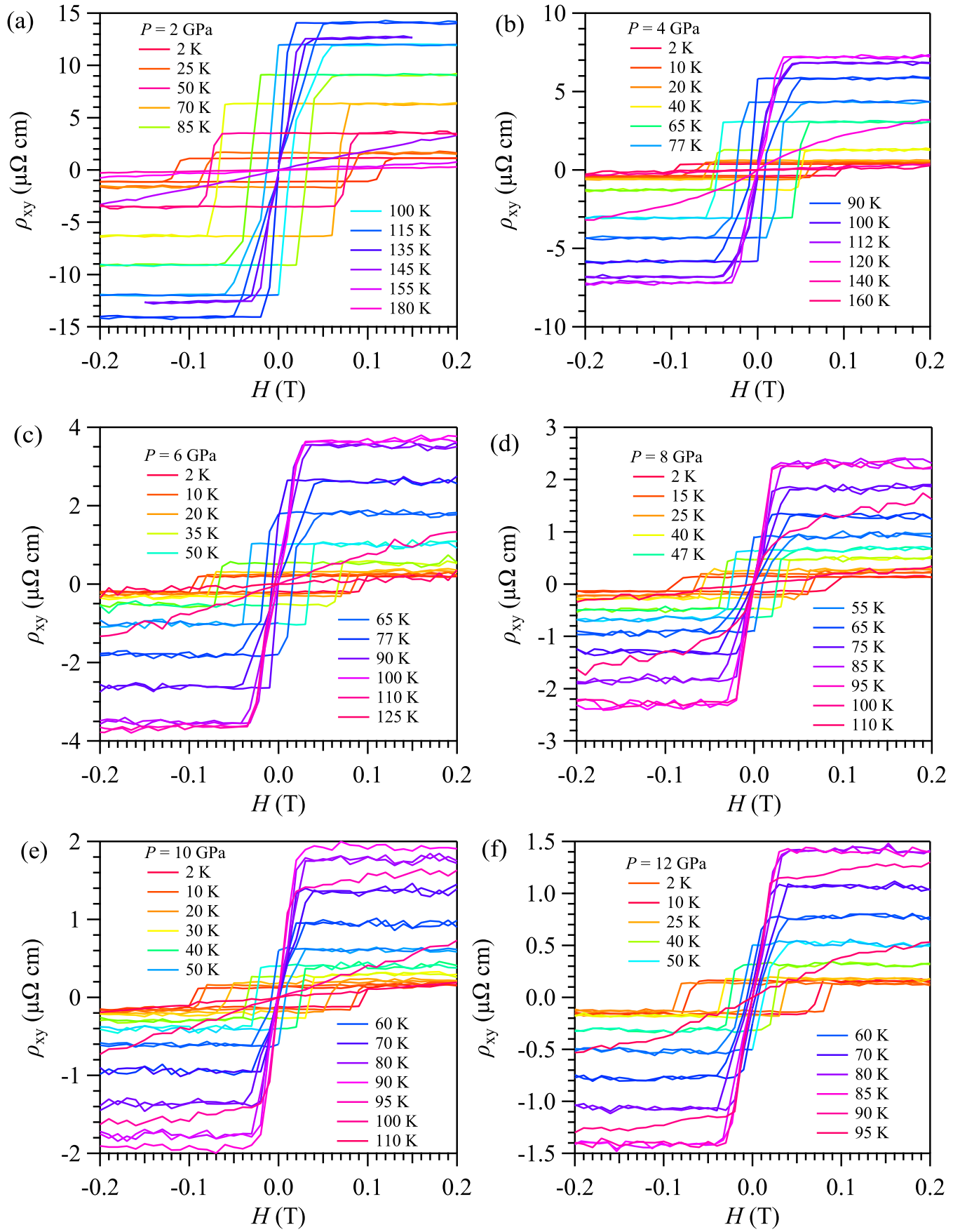

FIG. 2. Field dependence of Hall resistivity $\rho_{xy}(H)$ of $Co_3Sn_2S_2$ at various temperatures and pressures up to 12 GPa for H // c axis, respectively.

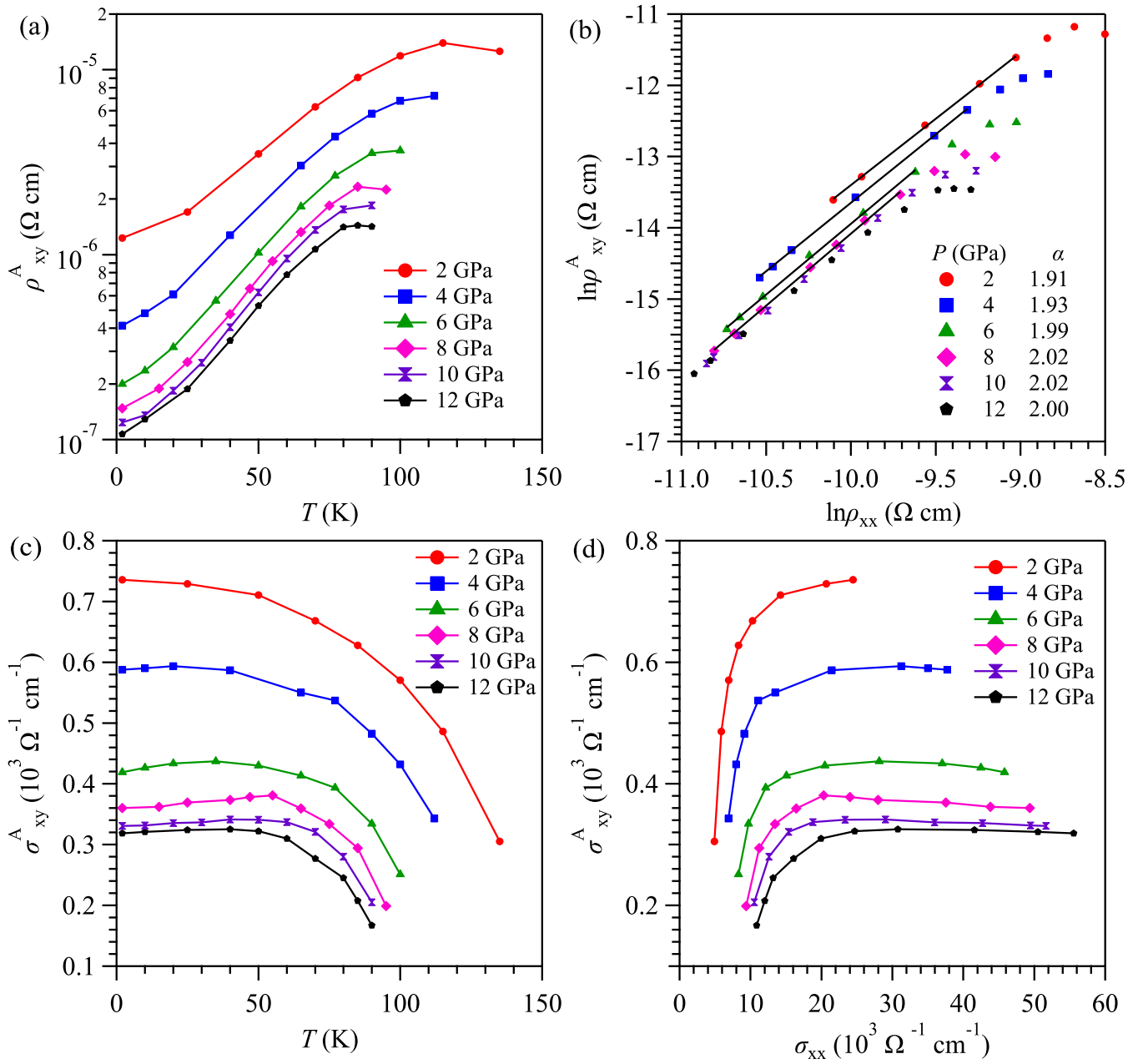

FIG. 3. Anomalous Hall effect of $Co_3Sn_2S_2$ under various pressures up to 12 GPa. (a) Temperature dependence of the anomalous Hall resistivity $\rho_{xy}{}^{A}$. (b) ln $\rho_{xy}{}^{A}$ as a function of ln ρ_{xx}. The solid lines are the linear fitting curves to get the coefficient α from $\rho_{xy}{}^{A} \propto \rho^{\alpha}{}_{xx}$. (c) Temperature dependence of the anomalous Hall conductivity $\sigma_{xy}{}^{A}$ at zero magnetic field. (d) $\sigma_{xy}{}^{A}$ as a function of the conductivity σ_{xx}.

these observations are expected for the AHE arising from the intrinsic mechanism dominated by the Berry curvature in momentum space [7,23,24,36].

In addition to a large anomalous Hall conductivity, $Co_3Sn_2S_2$ also features a giant anomalous Hall angle, which is characterized by the ratio of $\sigma_{xy}{}^{A}/\sigma_{xx} \sim 20\%$ at ambient pressure [23]. We thus calculated the anomalous Hall angle at different temperatures and pressures. Figure 4(a) displays the temperature dependences of $\sigma_{xy}{}^{A}/\sigma_{xx}$ at 2 GPa as an example. The data at other pressures are given in Fig. S1 of Supplemental Material Ref. [48]. As can be seen, $\sigma_{xy}{}^{A}/\sigma_{xx}$ at 2 GPa increases with temperature and reaches a maximum value of ~8.5% at $T^{peak} \sim 110$ K. In comparison with that at ambient pressure, the maximum value of $\sigma_{xy}{}^{A}/\sigma_{xx}$ at 2 GPa is significantly reduced, Fig. 4(b), but the reduction rate of $\sigma_{xy}{}^{A}/\sigma_{xx}$ tends to level off gradually upon further increasing pressure. Notably, the $\sigma^{A}{}_{H}/\sigma_{xx}$ still holds the relatively large value in a wide intermediate temperature range below T_C under each pressure, Fig. S1. Meanwhile, the T^{peak} decreases continuously with pressure, following a similar trend as $T_C(P)$ shown in Fig. 1(b).

It has been shown that the magnetic Weyl semimetal $Co_3Sn_2S_2$ hosts both a large anomalous Hall conductivity and a giant anomalous Hall angle at ambient pressure. To illustrate clearly the pressure effect on the AHE of $Co_3Sn_2S_2$, we have plotted the values of $\sigma_{xy}{}^{A}/\sigma_{xx}$ versus $\sigma_{xy}{}^{A}$ at different

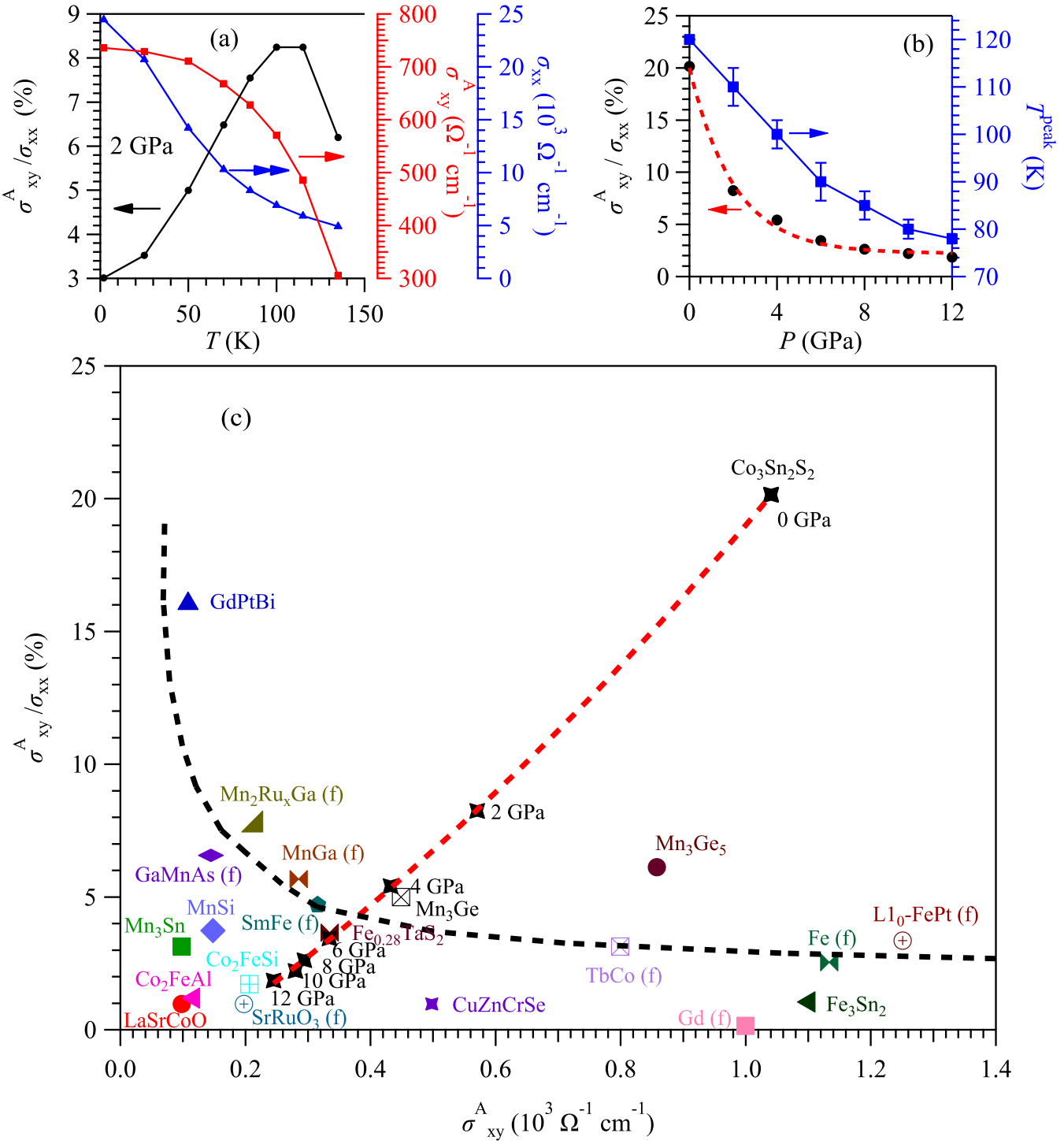

FIG. 4. (a) Temperature dependences of the anomalous Hall angle $\sigma_{xy}{}^A/\sigma_{xx}$, the charge conductivity σ_{xx} and the anomalous Hall conductivity $\sigma_{xy}{}^A$ of $Co_3Sn_2S_2$ at 2 GPa. (b) Pressure dependences of anomalous Hall angle $\sigma_{xy}{}^A/\sigma_{xx}$ and the peak temperature where the anomalous Hall angle reaches the maximum. (c) Comparison of our results and previously reported data on anomalous Hall angle $\sigma_{xy}{}^A/\sigma_{xx}$ as a function of anomalous Hall conductivity $\sigma_{xy}{}^A$. Lable (f) represents thin-film materials. The black and red dashed lines are guided to eyes.

pressures in Fig. 4(c) and compared with other AHE materials [23]. The magnetic materials below the black dashed line usually have topologically trivial band structure, which gives rise to a small $\sigma_{xy}{}^A/\sigma_{xx}$ due to the presence of comparable $\sigma_{xy}{}^A$ and σ_{xx}. It shows clearly in Fig. 4(c) that both $\sigma_{xy}{}^A/\sigma_{xx}$ and $\sigma_{xy}{}^A$ of $Co_3Sn_2S_2$ are reduced gradually with pressure and seems to enter the regime for typical AHE materials with trivial band topology at pressures above 4 GPa.

To further understand the pressure effects, we perform the theoretical calculations on its band structures, Weyl points (WPs) positions and intrinsic anomalous Hall conductivity by varying either magnetic moments (M) or lattice constants in our calculations in order to simulate the pressure effect.

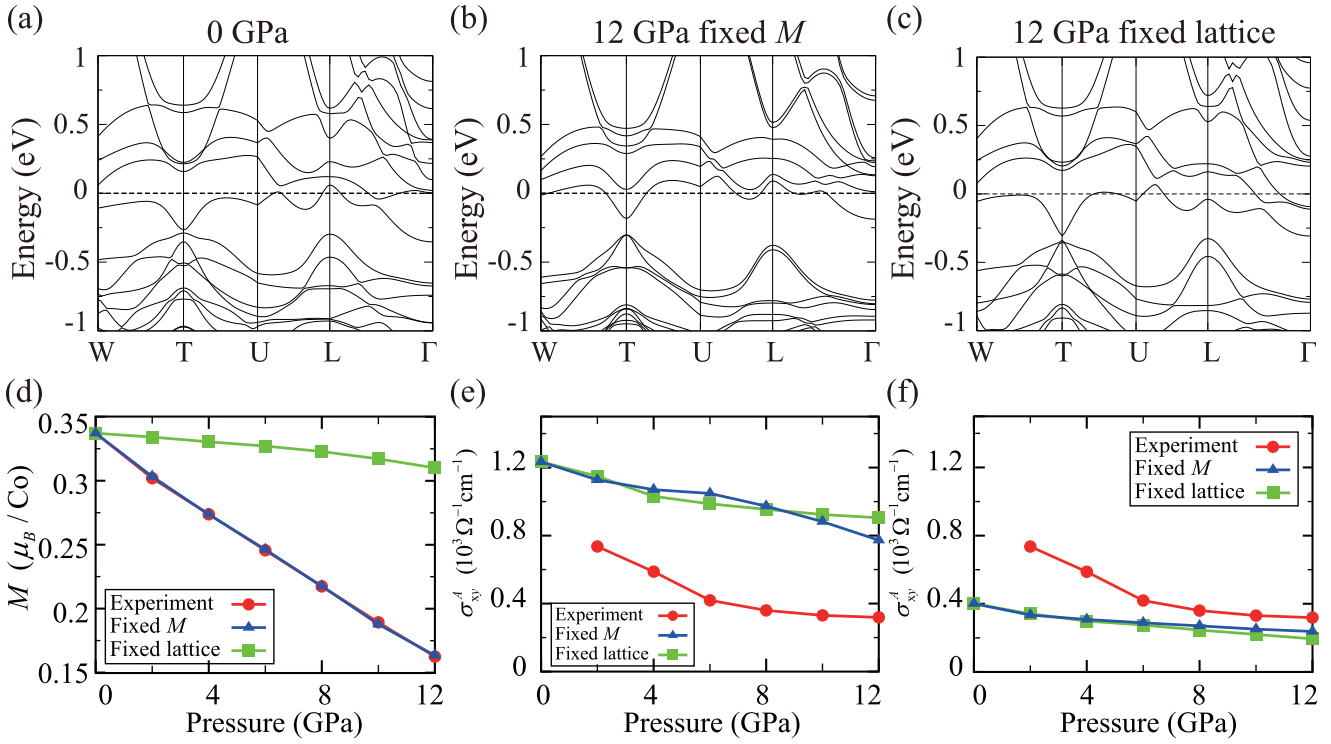

FIG. 5. The calculated band structures of $Co_3Sn_2S_2$ with SOC at (a) ambient pressure, (b) 12 GPa with fixed magnetic moments (fixed M) and (c) fixed lattice constants (fixed lattice). (d) The pressure dependent magnetic moments from experiments (Ref. [36]), fixed-M calculations, and fixed-lattice calculations. (e) The pressure dependent intrinsic AHC from experiments, fixed-M and fixed-lattice calculations. (f) The pressure dependent intrinsic AHC from experiments and from estimations based on the calculated WPs distances in the fixed-M and fixed-lattice calculations.

Hereafter, they are referred as fixed-M calculations and fixed-lattice calculations, respectively. For the former, the saturation M at different pressures are obtained by scaling the pressure-dependent magnetization values at the lowest temperature in Fig. 2(a) of Ref. [36] with respect to that at ambient pressure. As shown in Fig. 5(d), the saturation M decreases linearly from 0.33 μ_B at ambient to ~0.16 μ_B at 12 GPa. For the latter, the lattice constants at different pressures listed in Table S1 of Ref. [48] are extracted from the HP XRD results shown in Fig. 1 of Ref. [36].

First, we present the results of fixed-M calculations at different pressures. The calculated SOC band structures at 0 and 12 GPa are shown in Figs. 5(a) and 5(b). All calculated band structures from 0 to 12 GPa are given in Fig. S2 of Ref. [48]. With pressure increasing (magnetic moment decreasing), the band splitting between spin-up and spin-down channels is gradually suppressed, while the bandwidth of the same spin channel has little change [29], especially at the L point. This is obvious that the bandwidth is proportional to the hopping of electrons among atomic sites and determined by bond length and bond angle, which are not altered in fixed-M simulation. As shown in Fig. 5(e), the calculated intrinsic anomalous Hall conductivity at Fermi energy (blue triangle) decreases almost linearly with increasing pressure, which has the similar evolution as our experimental observations (read circle). Our results are also in good agreement with previous calculations based on the magnetic moments [23,24]. In addition, we also calculate the precise WPs positions, and find that the three pairs of WPs with opposite chirality related by inversion symmetry in the first BZ are close to each other. The anomalous Hall conductivity can be estimated via the formula $\sigma_{xy}{}^{A} = Ke^2/4\pi^2$, where K is the sum of distances along the direction of magnetization of three pairs of WPs related by inversion symmetry [2]. The estimated results shown in Fig. 5(f) exhibit a generally consistent trend with the first-principles calculations and the experiments results. But the smaller magnitude may be attributed to the facts that the WPs exist about 0.06 eV above the Fermi energy, and the contributions of other Fermi surfaces are ignored in the estimated results. Moreover, we also calculate the Fermi energy dependent intrinsic anomalous Hall conductivity, as shown in Fig. S4(a) of Ref. [48], and a similar decreasing trend with increasing pressure is also revealed.

For the fixed-lattice calculations, the calculated SOC band structure at 12 GPa is shown in Fig. 5(c) as a representative example, and all the others are given in Fig. S3 of Ref. [48]. Here, the application of HP mainly broadens up the bandwidth of the same spin channel, while the band splitting between spin-up and spin-down channels is hardly affected [36], especially at the L point. As such, the calculated magnetic moment (green square) in Fig. 5(d) is only reduced marginally with increasing pressure from 0.33 to ~0.3 μ_B, which is significantly smaller than that observed experimentally [36]. However, the calculated anomalous Hall conductivity (green square) at Fermi energy is decreasing gradually with a similar magnitude as that obtained from fixed-M calculations (blue triangle), Fig. 5(e). Here, it should be noted that the WPs positions are influenced by two factors under high pressures;

i.e. although pressure reduces the distance of a pair of WPs in fraction coordinate in BZ, the volume of BZ is enlarged by pressure. In total, the distance of a pair of WPs is found to decrease with increasing pressures, and so does the intrinsic anomalous Hall conductivity, Fig. 5(f). Similarly, the Fermi energy dependent intrinsic anomalous Hall conductivity also decreases with pressure as shown in Fig. S4(b) of Ref. [48].

Although our first-principles calculations on $Co_3Sn_2S_2$ by varying either magnetic moments or lattice constants show different evolutions of the band structures, the calculated distance between pairs of WPs and intrinsic anomalous Hall conductivity display similar declining trends, Figs. 5(e) and 5(f), which are in general consistent with our experiment results. The distinct evolutions of band structures noted above indicates that the FM order induced band splitting plays an essential role in determining the anomalous transport properties in the spin-polarized semimetal state of $Co_3Sn_2S_2$.

Finally, our present work also demonstrates that the AHE of magnetic Weyl semimetals are tunable. Reversibly, for example, the anomalous Hall conductivity and anomalous Hall angle of $Co_3Sn_2S_2$ might be enhanced if we can enhance its ferromagnetism by apply a negative pressure or tensile stress via employing strain devices or fabricating thin films on proper substrate [49].

IV. CONCLUSION

In summary, our present study demonstrates that the large intrinsic AHE in magnetic Weyl semimetal $Co_3Sn_2S_2$ can be tuned by pressure through modifying the ferromagnetism. We found that the application of high pressure can not only lower the ferromagnetic transition T_C, but also reduce monotonically the anomalous Hall conductivity ${\sigma_{xy}}^A$ and anomalous Hall angle ${\sigma_{xy}}^A/\sigma_{xx}$. The quadratic dependence of ${\rho_{xy}}^A \propto {\rho_{xx}}^2$ and the nearly independence of ${\sigma_{xy}}^A \sim \sigma_{xx}$ demonstrate that the intrinsic mechanism due to Berry curvature still dominates the AHE under high pressure. In combination of first-principles calculations, our work indicates that the distance between Weyl points with opposite chirality is substantially reduced accompanying the suppression of ferromagnetism in $Co_3Sn_2S_2$ under high pressure, thus providing an experimental route to tune the large AHE via modifying the nontrivial band topology of magnetic Weyl semimetals.

ACKNOWLEDGMENTS

This work is supported by the National Key R&D Program of China (2018YFA0305700), the National Natural Science Foundation of China (11904391, 11921004, 11925408, 11674369, 11888101, 11834016, and 11874400), the Beijing Natural Science Foundation (Z190008), the Strategic Priority Research Program and Key Research Program of Frontier Sciences of the Chinese Academy of Sciences (XDB25000000 and QYZDB-SSW-SLH013), as well as the CAS interdisciplinary team (JCTD-2019-01). J.P.S. acknowledge support from the China Postdoctoral Science Foundation and the Postdoctoral Innovative Talent program.

[1] X. L. Qi and S. C. Zhang, Rev. Mod. Phys. **83**, 1057 (2011).
[2] A. A. Burkov, Phys. Rev. Lett. **113**, 187202 (2014).
[3] R. S. K. Mong, A. M. Essin, and J. E. Moore, Phys. Rev. B **81**, 245209 (2010).
[4] Y. Ominato, A. Yamakage, and K. Nomura, J. Phys. Soc. Jpn. **88**, 114701 (2019).
[5] M. M. Otrokov, T. V. Menshchikova, I. P. Rusinov, M. G. Vergniory, V. M. Kuznetsov, and E. V. Chulkov, JETP Lett. **105**, 297 (2017).
[6] K. Y. Yang, Y. M. Lu, and Y. Ran, Phys. Rev. B **84**, 075129 (2011).
[7] N. Nagaosa, J. Sinova, S. Onoda, A. H. MacDonald, and N. P. Ong, Rev. Mod. Phys. **82**, 1539 (2010).
[8] Y. Tokura, K. Yasuda, and A. Tsukazaki, Nat. Rev. Phys. **1**, 126 (2019).
[9] D. Xiao, M. C. Chang, and Q. Niu, Rev. Mod. Phys. **82**, 1959 (2010).
[10] Z. Fang, N. Nagaosa, K. S. Takahashi, A. Asamitsu, R. Mathieu, T. Ogasawara, H. Yamada, M. Kawasaki, Y. Tokura, and K. Terakura, Science **302**, 92 (2003).
[11] S. V. Eremeev, M. M. Otrokov, and E. V. Chulkov, J. Alloys. Compd. **709**, 172 (2017).
[12] M. M. Otrokov, T. V. Menshchikova, M. G. Vergniory, I. P. Rusinov, A. Yu Vyazovskaya, Y. M. Koroteev, G. Bihlmayer, A. Ernst, P. M. Echenique, A. Arnau, and E. V. Chulkov, 2D Mater. **4**, 025082 (2017).
[13] M. M. Otrokov, I. I. Klimovskikh, H. Bentmann, A. Zeugner, Z. S. Aliev, S. Gass, A. U. B. Wolter, A. V. Koroleva, D. Estyunin, A. M. Shikin, M. Blanco-Rey, M. Hoffmann, A. Y. Vyazovskaya, S. V. Eremeev, Y. M. Koroteev, I. R. Amiraslanov, M. B. Babanly, N. T. Mamedov, N. A. Abdullayev, V. N. Zverev, B. Büchner, E. F. Schwier, S. Kumar, A. Kimura, L. Petaccia, G. Di Santo, R. C. Vidal, S. Schatz, K. Kißner, C. H. Min, S. K. Moser, T. R. F. Peixoto, F. Reinert, A. Ernst, P. M. Echenique, A. Isaeva, and E. V. Chulkov, Nature (London) **576**, 416 (2019).
[14] B. Chen, F. Fei, D. Zhang, B. Zhang, W. Liu, S. Zhang, P. Wang, B. Wei, Y. Zhang, Z. Zuo, J. Guo, Q. Liu, Z. Wang, X. Wu, J. Zong, X. Xie, W. Chen, Z. Sun, S. Wang, Y. Zhang, M. Zhang, X. Wang, F. Song, H. Zhang, D. Shen, and B. Wang, Nat. Commun. **10**, 4469 (2019).
[15] Y. J. Deng, Y. J. Yu, M. Z. Shi, Z. X. Guo, Z. H. Xu, J. Wang, X. H. Chen, and Y. B. Zhang, Science **367**, 895 (2020).
[16] S. V. Eremeev, M. M. Otrokov, and E. V. Chulkov, Nano. Lett. **18**, 6521 (2018).
[17] Y. Gong, J. W. Guo, J. H. Li, K. J. Zhu, M. H. Liao, X. Z. Liu, Q. H. Zhang, L. Gu, L. Tang, X. Feng, D. Zhang, W. Li, C. L. Song, L. L. Wang, P. Yu, X. Chen, Y. Y. Wang, H. Yao, W. H. Duan, Y. Xu, S. C. Zhang, X. C. Ma, Q. K. Xue, and K. He, Chin. Phys. Lett. **36**, 076801 (2019).
[18] J. Li, Y. Li, S. Du, Z. Wang, B. L. Gu, S. C. Zhang, K. He, W. Duan, and Y. Xu, Sci. Adv. **5**, eaaw5685 (2019).

[19] C. Liu, Y. C. Wang, H. Li, Y. Wu, Y. X. Li, J. H. Li, K. He, Y. Xu, J. S. Zhang, and Y. Y. Wang, Nat. Mater. **19**, 522 (2020).

[20] J. Wu, F. Liu, M. Sasase, K. Ienaga, Y. Obata, R. Yukawa, K. Horiba, H. Kumigashira, S. Okuma, T. Inoshita, and H. Hosono, Sci. Adv. **5**, eaax9989 (2019).

[21] J. Q. Yan, Q. Zhang, T. Heitmann, Z. L. Huang, K. Y. Chen, J. G. Cheng, W. D. Wu, D. Vaknin, B. C. Sales, and R. J. McQueeney, Phys. Rev. Mater. **3**, 064202 (2019).

[22] S. Zhang, R. Wang, X. P. Wang, B. Y. Wei, H. Q. Wang, G. Shi, F. Wang, B. Jia, Y. P. Ouyang, B. Chen, Q. Q. Liu, F. J. Xie, F. C. Fei, M. H. Zhang, X. F. Wang, D. Wu, X. G. Wan, F. Q. Song, H. J. Zhang, and B. G. Wang, Nano Lett. **20**, 709 (2020).

[23] E. K. Liu, Y. Sun, N. Kumar, L. Muchler, A. Sun, L. Jiao, S. Y. Yang, D. Liu, A. Liang, Q. Xu, J. Kroder, V. Suss, H. Borrmann, C. Shekhar, Z. Wang, C. Xi, W. Wang, W. Schnelle, S. Wirth, Y. Chen, S. T. B. Goennenwein, and C. Felser, Nat. Phys. **14**, 1125 (2018).

[24] Q. Wang, Y. Xu, R. Lou, Z. Liu, M. Li, Y. Huang, D. Shen, H. Weng, S. Wang, and H. Lei, Nat. Commun. **9**, 3681 (2018).

[25] S. N. Guin, P. Vir, Y. Zhang, N. Kumar, S. J. Watzman, C. Fu, E. Liu, K. Manna, W. Schnelle, J. Gooth, C. Shekhar, Y. Sun, and C. Felser, Adv. Mater. **31**, 1806622 (2019).

[26] J. Corps, P. Vaqueiro, A. Aziz, R. Grau-Crespo, W. Kockelmann, J. C. Jumas, and A. V. Powell, Chem. Mater. **27**, 3946 (2015).

[27] M. A. Kassem, Y. Tabata, T. Waki, and H. Nakamura, Phys. Rev. B **96**, 014429 (2017).

[28] Q. N. Xu, E. K. Liu, W. J. Shi, L. Muechler, J. Gayles, C. Felser, and Y. Sun, Phys. Rev. B **97**, 235416 (2018).

[29] R. Yang, T. Zhang, L. Q. Zhou, Y. M. Dai, Z. Y. Liao, H. M. Weng, and X. G. Qiu, Phys. Rev. Lett. **124**, 077403 (2020).

[30] O. V. Yazyev, Nat. Phys. **15**, 424 (2019).

[31] W. Schnelle, A. Leithe-Jasper, H. Rosner, F. M. Schappacher, R. Pöttgen, F. Pielnhofer, and R. Weihrich, Phys. Rev. B **88**, 144404 (2013).

[32] M. Holder, Y. S. Dedkov, A. Kade, H. Rosner, W. Schnelle, A. Leithe-Jasper, R. Weihrich, and S. L. Molodtsov, Phys. Rev. B **79**, 205116 (2009).

[33] G. Li, Q. Xu, W. Shi, C. Fu, L. Jiao, M. E. Kamminga, M. Yu, H. Tüysüz, N. Kumar, V. Süß, R. Saha, A. K. Srivastava, S. Wirth, G. Auffermann, J. Gooth, S. Parkin, Y. Sun, E. K. Liu, and C. Felser, Sci. Adv. **5**, eaaw9867 (2019).

[34] D. F. Liu, A. J. Liang, E. K. Liu, Q. N. Xu, Y. W. Li, C. Chen, D. Pei, W. J. Shi, S. K. Mo, P. Dudin, T. Kim, C. Cacho, G. Li, Y. Sun, L. X. Yang, Z. K. Liu, S. S. P. Parkin, C. Felser, and Y. L. Chen, Science **365**, 1282 (2019).

[35] N. Morali, R. Batabyal, P. K. Nag, E. K. Liu, Q. N. Xu, Y. Sun, B. H. Yan, C. Felser, N. Avraham, and H. Beidenkopf, Science **365**, 1286 (2019).

[36] X. L. Chen, M. Y. Wang, C. C. Gu, S. Y. Wang, Y. H. Zhou, C. An, Y. Zhou, B. W. Zhang, C. H. Chen, Y. F. Yuan, M. Y. Qi, L. L. Zhang, H. D. Zhou, J. H. Zhou, Y. G. Yao, and Z. R. Yang, Phys. Rev. B **100**, 165145 (2019).

[37] J. G. Cheng, K. Matsubayashi, S. Nagasaki, A. Hisada, T. Hirayama, M. Hedo, H. Kagi, and Y. Uwatoko, Rev. Sci. Instrum. **85**, 093907 (2014).

[38] J. G. Cheng, B. S. Wang, J. P. Sun, and Y. Uwatoko, Chin. Phys. B **27**, 077403 (2018).

[39] G. Kresse and J. Furthmüller, Phys. Rev. B **54**, 11169 (1996).

[40] P. E. Blöchl, Phys. Rev. B **50**, 17953 (1994).

[41] G. Kresse and D. Joubert, Phys. Rev. B **59**, 1758 (1999).

[42] J. P. Perdew, J. A. Chevary, S. H. Vosko, K. A. Jackson, M. R. Pederson, D. J. Singh, and C. Fiolhais, Phys. Rev. B **46**, 6671 (1992).

[43] R. D. King-Smith and D. Vanderbilt, Phys. Rev. B **47**, 1651 (1993).

[44] A. A. Mostofi, J. R. Yates, G. Pizzi, Y.-S. Lee, I. Souza, D. Vanderbilt, and N. Marzari, Comp. Phys. Commun. **185**, 2309 (2014).

[45] Q. S. Wu, S. N. Zhang, H.-F. Song, M. Troyer, and A. A. Soluyanov, Comp. Phys. Commun. **224**, 405 (2018).

[46] K. Koyama, T. Goto, T. Kanomata, and R. Note, Phys. Rev. B **62**, 986 (2000).

[47] T. F. Smith, J. A. Mydosh, and E. P. Wohlfarth, Phys. Rev. Lett. **27**, 1732 (1971).

[48] See Supplemental Material at http://link.aps.org/supplemental/10.1103/PhysRevMaterials.4.044203 for details about the temperature dependences of anomalous Hall angles and conductivity at different pressures as well as the calculated band structures and anomalous Hall conductivity at different pressures.

[49] Z. Guguchia, I. J. Verezhak, D. Gawryluk, S. S. Tsirkin, J. X. Yin, I. Belopolski, H. Zhou, G. Simutis, S. S. Zhang, T. A. Cochran, G. Chang, E. Pomjakushina, L. Keller, Z. Skrzeczkowska, Q. Wang, H. C. Lei, R. Khasanov, A. Amato, S. Jia, T. Neupert, H. Luetkens, and M. Z. Hasan, Nat. Commun. **11**, 559 (2020).